

STUDY OF MAGNETIZATION AND CRITICAL TEMPERATURE FOR NANOMAGNETIC PARTICLES

By

ABRHAM FESEHA

SUBMITTED IN PARTIAL FULFILLMENT OF THE
REQUIREMENTS FOR THE DEGREE OF
MASTER OF SCIENCE IN PHYSICS
AT
ADDIS ABABA UNIVERSITY
ADDIS ABABA, ETHIOPIA
JUNE 2011

© Copyright by ABRHAM FESEHA , 2011

ADDIS ABABA UNIVERSITY
COLLEGE OF NATURAL SCIENCE
FACULTY OF CHEMICAL AND PHYSICAL SCIENCE
DEPARTMENT OF PHYSICS

The undersigned here by certify that they have read and recommend to the School of Graduate Studies for acceptance a thesis entitled "**STUDY OF MAGNETIZATION AND CRITICAL TEMPERATURE FOR NANOMAGNETIC PARTICLES** " by **ABRHAM FESEHA** in partial fulfillment of the requirements for the degree of **Master of Science in Physics**.

Dated: JUNE 2011

Approved by the examination commitee

Prof. P.Singh, advisor: _____

Dr. Chernet Amente, Examiner: _____

Prof. Javed Mazher, Examiner: _____

ADDIS ABABA UNIVERSITY

Date: **JUNE 2011**

Author: **ABRHAM FESEHA**

Title: **STUDY OF MAGNETIZATION AND CRITICAL TEMPERATURE FOR NANOMAGNETIC PARTICLES**

Department: **Physics**

Degree: **M.Sc.** Convocation: **JUNE** Year: **2011**

Permission is herewith granted to Addis Ababa University to circulate and to have copied for non-commercial purposes, at its discretion, the above title upon the request of individuals or institutions.

Signature of Author

THE AUTHOR RESERVES OTHER PUBLICATION RIGHTS, AND NEITHER THE THESIS NOR EXTENSIVE EXTRACTS FROM IT MAY BE PRINTED OR OTHERWISE REPRODUCED WITHOUT THE AUTHOR'S WRITTEN PERMISSION.

THE AUTHOR ATTESTS THAT PERMISSION HAS BEEN OBTAINED FOR THE USE OF ANY COPYRIGHTED MATERIAL APPEARING IN THIS THESIS (OTHER THAN BRIEF EXCERPTS REQUIRING ONLY PROPER ACKNOWLEDGEMENT IN SCHOLARLY WRITING) AND THAT ALL SUCH USE IS CLEARLY ACKNOWLEDGED.

Table of Contents

Table of Contents iii

List of Tables iv

List of Figures v

Acknowledgements vii

Abstract viii

Introduction 1

1 General Introduction to Nanomagnetic particles 3
- 1.1 Nanomagnetism . . . 3
- 1.2 The Origin of Nanomagnetic Behavior . . . 4
  - 1.2.1 Broken Translation Symmetry . . . 5

2 Review on Study Of Magnetization and Critical Temperature For Nanomagnetic particles 13
- 2.1 Fine Particles Superparamagnetism . . . 13
  - 2.1.1 Magnetic Materials and Nanomagnetism . . . 13
  - 2.1.2 Superparamagnetism . . . 18
  - 2.1.3 Relaxation Time . . . 19
  - 2.1.4 Blocking Temprature (T_B) . . . 20
- 2.2 The Importance Of Nanomagnetism . . . 22

3 Mathematical Calculation of Nanomagnetic Parameters 26
- 3.1 Critical Behavior Of Pure Ferromagnetic Nanoparticles . . . 26
  - 3.1.1 Theoretical Model . . . 27
  - 3.1.2 Coordination number . . . 34
  - 3.1.3 $T_C(D)$ of Pure nanoparticles . . . 35
  - 3.1.4 Graphic Representation Of $T_C(D)$ . . . 37

4 Result and Conclusion 42

List of Tables

3.1 Theoretical and Experimental values [22,23] of $T_C(D)$,Z_{eff} and Z_{eff}/Z for different values of D 39

List of Figures

1.1 Density of electronic states D(E) as a function of energy for electrons, from bottom to top, in zero dimension, in one dimension, two dimensions, and three dimensions (Based on [10]) 7

1.2 Graph of E/E_0 (dotted lines) for the lower three energy levels and wavefunctions vs. x (continuous lines) for a free electron gas confined to a one-dimensional box 8

1.3 Normalized densities of electronic states $D(E)/C_p$ (where C_p is a constant factor for each dimensionality p) as a function of energy, for different dimensionalities 9

2.1 Magnetization versus field ($Mvs.H$) curves for (a) an assembly of ferromagnetic nanoparticles and (b) an assembly of superparamagnetic nanoparticles. 14

2.2 Hysteresis loops (magnetization versus applied magnetic field strength) characteristic of ferromagnetic and super paramagnetic nanoparticles. . . . 15

2.3 Temperature variation of the relaxation time and of critical diameter for spherical cobalt particles. 21

2.4 Evolution of magnetic recording: hard disk areal density in gigabits per square inch as a function of the year in which the products became available in the market [13]. (Reprinted from [11] with permission from IBM Technical Journals) 23

2.5 The concept of the magnetic tunnel junction 24

2.6 The principle of the TMR effect. For the antiferromagnetic configuration of the magnetic layers $R_{AFM} \gg R_{FM}$ 25

2.7 Courtesy of Tom Arny, Explorations 25

3.1 Size dependence of the effective (Eq.(3.1.17)) . Particle diameter D is given in units of the lattice parameter b. 32
3.2 34
3.3 (Color online) Particle with diameter D =10 having 1067 atoms, bcc structure, and an average coordination number $\langle z \rangle = 6.96$. Surface atoms with 4, 5, 6 and 7 nearest neighbors are colored green, blue, red, and yellow, respectively 35
3.4 Particle size dependence of the reduced critical temperature for pure ferromagnetic nanoparticles with z=8 ,according to Eqs.(3.1.28) 37
3.5 Effective coordinate number versus Diameter 40
3.6 $T_C(D)$ versus Diameter 41
3.7 $T_C(D)$ versus Diameter 41

Acknowledgements

First thanks God for providing me the blessings to complete this work. Next I would like to express my sincere thanks for my advisor and instructor Prof. P.Singh for his guidance, assistance, supervision and contribution of valuable suggestions. His scientific excitement, integral view on research and overly enthusiasm, has made a deep impression on me. I would like to thank to my family and all friends for providing encouragement and support.

Abstract

Magnetic nanostructures, such as dots and dot arrays, nanowires, multilayers and nanojunctions, are reviewed and compared with bulk magnets. By using the Gibbs free energy variational principle based on the Bogoliubov inequality the magnetic properties and critical behavior of metallic nanoparticles having concurrently atomic disorder, dilution and competing interactions, are studied within the framework of an Ising model. As a case of study we have considered the $Fe_{0.5}Mn_{0.1}Al_{0.4}$ alloy characterized for exhibiting, under bulk conditions, low temperature reentrant spin glass (RSG) behavior and for which experimental and simulation results are available. Our results allow concluding that the variational model is successful in reproducing features of the dependence of the critical temperature with particle size and low temperature magnetization reduction consistent with a RSG behavior. In this work we compute the magnetization per site and the magnetic susceptibility, as a function of temperature, for different values of the coordination number.

Introduction

The use of magnetism and magnetic materials has a long history. Ancient Chinese made use of lodestones as magnetic compasses for navigation. Scientific understanding of magnetism can be traced back to the 17^{th} century with pioneering work done by Gilbert [1]. Classical electromagnetism was summarized as Maxwells equations [3] at the end of the 19th century. A better understanding of magnetism came with the birth of quantum mechanics at the beginning of the 20^{th} century and the realization that the electron has an intrinsic spin and magnetic moment. Detailed models of the microscopic structure of magnetic materials were then constructed by scientists like Stoner, Weiss and Bloch [4,5].

Today, the study of magnetism has come to a new stage nanomagnetism. With the development of nanoscience and nanotechnology, magnetic structures with length scales ranging from a few inter-atomic distances to one micron have attracted intense research interests in the past few decades [6-8]. The scientific and technological importance of magnetic nanostructures is due to three main reasons. Firstly, there is an overwhelming variety of structures with interesting physical properties, ranging from naturally occurring nanomagnets to artificial nanostructures. Secondly, the involvement of nanoscale effects in the explanation and improvement of the properties of advanced magnetic materials. Thirdly, the study of magnetic nanostructures has led to completely new research areas like spintronics. Though nanomagnetism started only a few decades ago it has now evolved into a well-established branch of condensed matter physics.

The layout of the paper is as follows. In Sec. I and Sec. II we describe the theoretical model. In Sec. III we present our numerical results. This section provides finite-size scaling analysis of both pure ferromagnetic nanoparticles , and $Fe_{0.5}Mn_{0.1}Al_{0.4}$ nanoparticles from the standpoint of the free energy variational principle based on the Bogoliubov inequality approaches. Result and Conclusions are finally presented in Sec. IV.

Chapter 1

General Introduction to Nanomagnetic particles

1.1 Nanomagnetism

The objects of study of Nanoscience are the phenomena involving objects of dimensions usually in the range from 1 ($1nm = 10^{-9}m$) to 100 nm. This is the range of sizes of many molecules and viruses, and is also the characteristic length scale of many physical processes. The lateral dimensions of present-day integrated circuit components, as well as the dimensions of grains in magnetic-recording film media, are contained in this range.

Nanomagnetism is the area of research in physics, which deals with the magnetic properties of objects that have at least one dimension in the nanoscopic range. Nanomagnetism includes in its scope the study of properties and applications of the magnetism of isolated nanoparticles, nanodots, nanowires, thin films and multilayers, and also macroscopic sam ples that contain nanoscopic particles. Materials that contain particles, films, and other structures in the nanometric scale are often described as nanostructured materials.

Objects with dimensions from 100 to 1,000 nm are usually described as meso-scopic; although our focus in the present work is on magnetic properties of objects of nanoscopic dimension, we will also consider the behavior of objects of mesoscopic size.

1.2 The Origin of Nanomagnetic Behavior

The emergence of the new phenomena that are the object of nanomagnetism has its origin in the fact that the magnetism of samples of nanoscopic or mesoscopic sizes presents important differences compared to the magnetism of macroscopic samples. One could describe these differences, in a simplified way, as arising from the fact that the magnetic systems of nanoscopic or mesoscopic scales present: (1) dimensions comparable to characteristic lengths, such as the limiting size of magnetic domains; (2) broken translation symmetry, which results in sites with reduced coordination number, with broken exchange bonds and frustration. Also, nanoscopic or mesoscopic objects exhibit a higher proportion of surface (or interface) atoms.

Another factor that modifies the magnetic properties of the nanoobjects is that they are in general in close contact with other physical systems, for example, with a substrate or a capping layer, in the case of most thin films and multilayers. In the case of nanoparticles, these objects may be immersed in solid matrices, or compacted in a container: in both cases, each particle may feel a strong interaction with its immediate neighborhood.

Also, in general, as systems such as ensembles of nanoparticles are prepared with smaller dimensions, the presence of imperfections and defects becomes more relevant, making the obtention of identical sets of nanoobjects more difficult. Often the properties of the nanoscopic objects have to be derived from samples formed of ensembles of such objects. The spin wave spectra of samples of nanoscopic dimensions are also modified (e.g., [16]). The dispersion relation for spin waves for wavelengths longer than the lattice spacing is $\hbar\omega = D\kappa^2$, where D is the stiffness constant, and k is the magnitude of the spin wavevector. For a spin wave energy comparable to the thermal energy, one has $k \approx (k_B T/D)^{1/2}$, where k_B is the Boltzmann constant. For Fe, $D(4.2K) \approx 3\text{meV}nm^2$ and the corresponding length $L = 1/k \approx 3$ nm at liquid helium temperature, which implies that spin wave spectra of nanoscopic objects are significantly modified, if compared to those of bulk

samples.

The dynamic behavior of magnetic objects of nanometric size also differs from the behavior of macroscopic samples of the same constituents. The main cause for this difference is the enhanced importance of thermal fluctuations under the usual experimental conditions. The phenomenon of superparamagnetism is observed in mag- netic nanoparticles if the thermal energy k_BT is of the same order-of-magnitude of the anisotropy energy of the particles, leading to an effectively zero measured magnetic moment. The superparamagnetism of nanoparticles is discussed in Sect.2.1.2 (p. 18).

1.2.1 Broken Translation Symmetry

Every finite crystal has frontiers, where the translational symmetry is lost or broken. In solids of nanometric size a significant proportion of the atoms are on or near these frontiers. The absence of translation symmetry brings about several important consequences to the physical properties of these systems.

Three aspects of the problem of symmetry breaking will be discussed: (1) the relation of the physical properties of the samples to their dimensionality (samples with quasi-zero dimension (0D), unidimensional (1D), bidimensional (2D) or tridimensional (3D)); (2) the change in coordination of the atoms at the interface, and (3) the effect of the increase in the proportion of surface (or interface) atoms in nanoscopic samples.

Dimensionality and Density of Electronic States

The electronic band structure of a solid depends on its dimensionality. This can be exemplified in the simplest description of a conducting solid, the free electron model, in which the electrons are treated as a gas (called a Fermi gas) only subject to the infinite potentials at the walls of the container. An electron gas in a limited spatial region will show an availability of electronic states (measured by its density of states D(E)) that depends on the dimensionality of this region: if it is in one dimension or two dimensions, D(E) will differ from the three-dimensional case. The effects of the difference in dimensionality

may be shown through the differences in D(E), and are summarized in Fig. 1.1.

Let us examine initially a Fermi gas in three dimensions; we wish to obtain the form of the density of states D(E). The electrons are supposed to be in a container with three dimensions and infinitely high walls; there are no interactions between the electrons.

Let us consider that the potential V (x, y, z) inside the box of side L is V_0 =const for $0 \leq x \leq L$,$0 \leq y \leq L$, and $0 \leq z \leq L$; $V = \infty$ otherwise. The time-independent Schrdinger equation will be

$$\frac{-\hbar^2}{2m}\nabla^2\Psi(r) + V(r)\Psi(r) = E'\Psi(r) \tag{1.2.1}$$

Using $E = E^{'} - V_0(r)$ one obtains

$$\frac{-\hbar^2}{2m}\nabla^2\Psi(r) = E\Psi(r) \tag{1.2.2}$$

Since the infinite potential at the walls forbids the presence of the electrons out- side them, the boundary conditions for $\Psi(r)$ will be: $\Psi = 0$ for $x = 0$ and $x = L$, $y = 0$ and $y = L$ and $z = 0$ and $z = L$.

The solution of Schrdingers equation, using these boundary conditions, will be:

$$\Psi(r) = \left(\frac{2}{L}\right)^{\frac{3}{2}} sink_x x sink_y y sink_z z \tag{1.2.3}$$

The corresponding energies are obtained by substituting $\Psi(x)$ from (1.2.3) into (1.2.2):

$$E = \frac{\hbar^2}{2m}(k_x^2 + k_y^2 + k_z^2) \tag{1.2.4}$$

where m is the electron mass and k_i are the components of its wavevector. From the boundary conditions, one obtains

$$k_x = \pm\frac{2\pi}{L}n_x, k_y = \pm\frac{2\pi}{L}n_y, k_z = \pm\frac{2\pi}{L}n_z \tag{1.2.5}$$

where n_x ,n_y and n_z take values 1,2,3,...

The wave functions for a free electron in a one-dimensional box, for the first three values of n, and the corresponding energies E are illustrated in Fig. 1.2. This figure

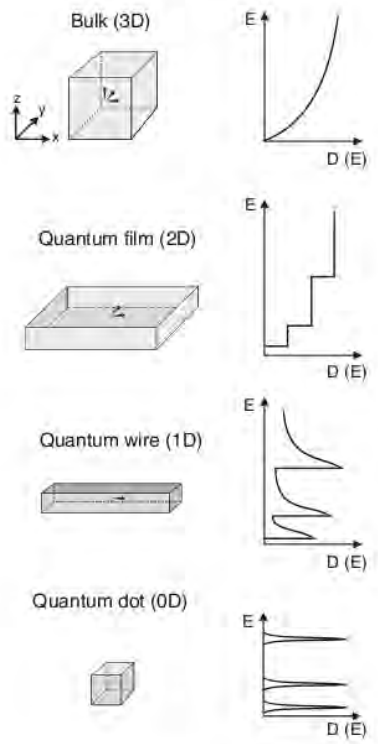


Figure 1.1: Density of electronic states D(E) as a function of energy for electrons, from bottom to top, in zero dimension, in one dimension, two dimensions, and three dimensions (Based on [10])

shows the form of the first three lowest energy wave functions, as well as the corresponding energies E/E_0 where E_0 is the energy for the level with $n = 1$. According to the Pauli exclusion principle, two electrons (spin up and spin down) occupy one state defined by (n_x , n_y , n_z). But how many states are there to be occupied? To count the number of states, one has to count the number of values of k.

At $T = 0K$, all states are occupied up to k_F , the Fermi wavevector, in a volume $V_k = \left(\frac{4}{3}\pi k_F^3\right)$. Since each triplet (k_x, k_y, k_z) occupies a volume of $\nu = (2\pi/L)^3$ in k-space,the number of states N will be

$$2 \cdot \frac{V_k}{\nu} = 2 \cdot \frac{\frac{4}{3}\pi k_F^3}{(\frac{2\pi}{L})^3} = \frac{V}{3\pi^2} k_F^3 = N \tag{1.2.6}$$

where V is the volume occupied by the electrons in real space.

From this equation one derives k_F , and substituting into the expression of the energy

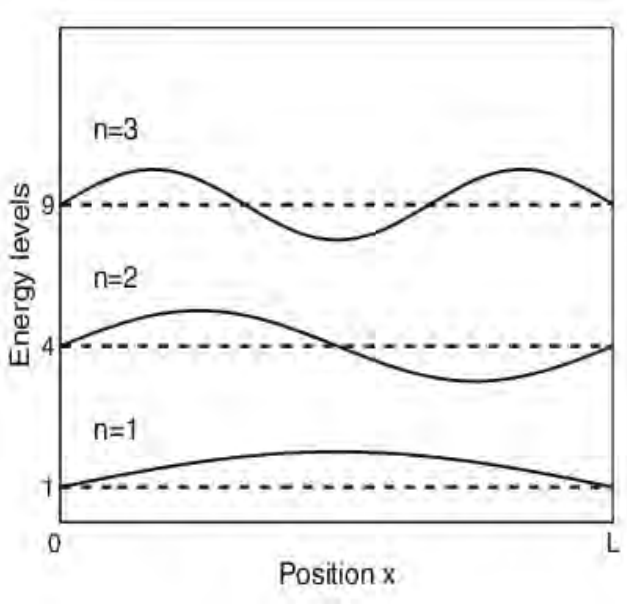


Figure 1.2: Graph of E/E_0 (dotted lines) for the lower three energy levels and wave-functions vs. x (continuous lines) for a free electron gas confined to a one-dimensional box

(1.2.4), one obtains the Fermi energy E_F :

$$E_F = \frac{\hbar^2}{2m}\left(\frac{3\pi^2 N}{V}\right)^{\frac{2}{3}} \tag{1.2.7}$$

This allows writing N as a function of E_F . The derivative of the expression obtained for N is the density of electron states at the Fermi level $D(E_F)$

$$D(E_F) \equiv \frac{dN}{dE_F} = \frac{V}{2\pi^2}\left(\frac{2m}{\hbar^2}\right)^{\frac{3}{2}} {E_F}^{1/2} \tag{1.2.8}$$

This result is the density of electron states at the Fermi level for the free electron gas contained in a three-dimensional box. The two-dimensional and the one- dimensional densities of states may be derived, using in (1.2.6) the corresponding expressions for the volume of the box, total volume in k-space V_k and volume per point in k-space in two and one dimensions. In two dimensions, $V_k = \pi k^2$, the volume per point is $(2\pi/L)^2$and the volume of the box is L^2 . In one dimension, the total volume in k-space is $V_k = 2k$, the volume per point is $(2\pi/L)$ and the volume of the box is L. Consequently, the general expression for the density of states is

$$D(E) = \left(\frac{2m}{\hbar^2}\right) \frac{V_K}{\nu} \frac{P}{K^2} \tag{1.2.9}$$

where p = 1, 2, 3 are the corresponding dimensionalities, as can be easily verified. Substituting, one obtains the densities of states $D(E)$, for the different dimensionalities.

In three dimensions:

$$D(E) = V \frac{1}{2\pi^2} \left(\frac{2m}{\hbar^2}\right)^{3/2} E^{1/2} \tag{1.2.10}$$

In two dimensions,

$$D(E) = V \frac{1}{2\pi} \left(\frac{2m}{\hbar^2}\right) \tag{1.2.11}$$

Note that in this case the density of states D(E) does not depend on the energy, it is a constant.

And finally, in one dimension,

$$D(E) = V \frac{1}{\pi} \left(\frac{2m}{\hbar^2}\right)^{1/2} E^{-1/2} \tag{1.2.12}$$

These expressions for the densities of states of the free electron gas for different dimensions (1, 2, and 3) are represented in the graphs of Fig. 1.3.

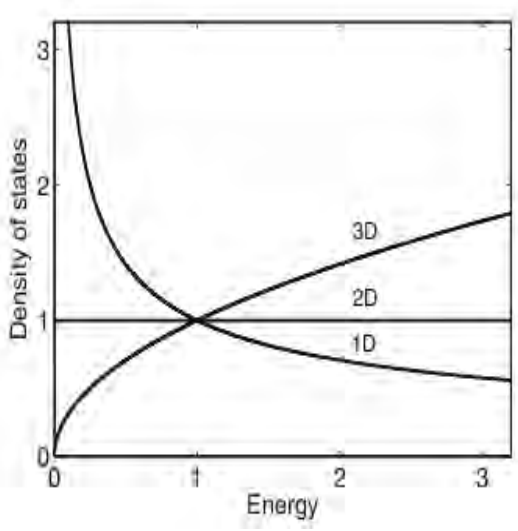


Figure 1.3: Normalized densities of electronic states $D(E)/C_p$ (where C_p is a constant factor for each dimensionality p) as a function of energy, for different dimensionalities

We will now discuss what happens if the object that contains the electrons is a solid of nanometric dimensions. There will be quantum confinement in any case where one or more dimensions of the volume that contains the electron gas are comparable to the Fermi wavelength $\lambda_F = 2\pi/k_F$ of the electron. In objects with dimensions comparable to this wavelength the wave character of the electrons will be dominant, and their energies will be quantized. To obtain the densities of states in the confined systems, one has to take into consideration the boundary conditions. The electrons may be confined in the three dimensions, i.e., they may be contained in an object that is nanometric in the three dimensions this is the case of a quantum dot. If the electrons are confined in two dimensions, i.e., if the third dimension is macroscopic, one has a quantum wire, or a nanowire. If the electrons are confined in one dimension, one has a quantum well, or a quantum film. If the electrons are not confined in any dimension, one has a macroscopic object.

1. Object confined in three dimensions (quantum dot):

The allowed values for the energy of the electrons are given by (1.2.4). The energies of the different levels depend on k_x , k_y , and k_z. The condition of infinite potential at the walls implies $k_x = n_x\pi/L_x$,$k_y = n_y\pi/L_y$ and $k_z = n_z\pi/L_z$, where L_x , L_y and L_z are the dimensions of the box where the electrons are contained.

$$E = \frac{\hbar^2\pi^2}{2m}\left(\frac{n_x^2}{L_x^2} + \frac{n_y^2}{L_y^2} + \frac{n_z^2}{L_z^2}\right) \tag{1.2.13}$$

The separation between the energy levels is given by dE_k . One assumes to simplify $L_x = L_y = L_z = L$, and also $n_x = n_y = n_z = n$. For a nanoscopic solid with L = 1 nm, the energy levels are separated by $dE = 3\frac{\hbar^2\pi^2}{mL^2} \sim 1eV$. Therefore, the energy spectrum is formed of discrete levels, similar to the atomic levels, with energies given by

$$E_n = \frac{3\hbar^2\pi^2}{2mL^2}n^2 \tag{1.2.14}$$

2. Object confined in two dimensions, and free in one dimension (quantum wire or nanowire):

One may assume that the object is macroscopic in the z direction, and the dimensions $L_x = L_y$ are nanoscopic. From (1.2.13), taking $L_z = L$ and $n_z = n$ one obtains

$$E = \frac{\hbar^2\pi^2}{2m}\left(\frac{n_x^2}{L_x^2} + \frac{n_y^2}{L_y^2} + \frac{n^2}{L^2}\right) \tag{1.2.15}$$

In this case the separation between the energy levels labelled by n_x and n_y remains large, of the order of eV . The separation of the levels corresponding to n is much smaller, since L is a number typically 10^7–10^9 times larger than the x and y dimensions. One may consider these levels as occupying a practically continuous range of values. E(k) is then given by parabolas displaced by $\hbar^2\pi^2/2mL^2$.

The density of states curve D(E) is formed of a series of peaks at the values of E_n ; above each peak there exists a region with a continuous dependence with E.

3. Object confined in one dimension and free in two dimensions (quantum film or quantum well) :

If the confinement is limited to the x axis, the electrons are free to move in the directions of the plane (y and z axes) and the energy levels are given (for $L_y = L_z = L$) by

$$E = \frac{\hbar^2\pi^2}{2m}\left(\frac{n_x^2}{L_x^2} + \frac{2n^2}{L^2}\right) \tag{1.2.16}$$

In the same way as in the preceding case, the energies of the levels, labelled by n_x , exhibit a large difference. E vs. k_y and k_z is given by parabolic surfaces displaced of $\frac{\hbar^2\pi^2}{2mL^2}$. The density of states curve D(E) is formed of a series of steps, within a parabolic envelope.

4. Object without confinement, electrons free to move in the three directions (macroscopic object):

Taking the frontiers defined by $L_x = L_y = L_z = L$ as macroscopic lengths, the energies

are given by

$$E = \frac{\hbar^2 \pi^2}{2m} \left(3 \frac{n^2}{L^2} \right) \tag{1.2.17}$$

The energy levels are now distributed over a continuum of states, as shown in Fig. 1.3 The graph of E_K is represented by a parabolic surface and the density of states curve D(E) is the familiar parabola shown in Fig. 1.3.

The density of state curves shown in Fig. 1.1 differ from those that appear in Fig. 1.3, since there are obvious steps or discontinuities in Fig. 1.1. These steps arise, for example, in the case of a 2D solid (quantum film, or quantum well), from the electron confinement in the dimension perpendicular to the plane. This confinement induces the appearance of discrete levels in the density of states; the dependence D(E) = constant is observed at the energies corresponding to these levels.

A simple visual examination of the density of states curves D(E) shown in Fig. 1.1 reveals important differences in this function. The appearance of D(E) for the 0D sample is similar to the same function for atoms: D(E) has narrow peaks, corresponding to well-defined values of the kinetic energy of the conduction electrons. For this reason, quantum dots are often referred to as artificial atoms.

The curve D(E) for quantum wires (one-dimensional) also has narrow peaks, but in this case there are electronic states that may be occupied for intermediate values of the energy E. The curve for a two-dimensional nanosystem shows some well-defined steps, and again there exists a quasi-continuum of states that may be occupied in the whole range of energies. The result of D(E) for a macroscopic system in the free electron approximation is the well-known parabola, applicable in the simplest description of the metals.

Chapter 2

Review on Study Of Magnetization and Critical Temperature For Nanomagnetic particles

2.1 Fine Particles Superparamagnetism

2.1.1 Magnetic Materials and Nanomagnetism

A bulk ferromagnetic material displays a distinct nonlinear magnetic response to an applied magnetic field, referred to as a hysteresis loop or$Mvs.H$ curve (Figure 2.1). Despite a ferromagnets characteristic spontaneous internal magnetic moment, without an applied field the magnetization is usually zero, that is, the $Mvs.H$ curve starts at the origin. This is because in order to minimize the magnetostatic energy within a bulk ferromagnet, magnetic domains-small regions of magnetic alignment are formed. When a magnetic field is applied, the energy of the field can overcome the magnetostatic energy associated with the domain formation, and the magnetization of the material increases until all of the moments are aligned with the field. The magnetic alignment with the field occurs in two ways: (1) the walls that make up the domains can shift resulting in the growth of domains already aligned with the field at the expense of those not aligned, and (2) the rotation of the magnetization vector away from one crystallographic axis and toward the field. The final magnetization associated with the complete alignment of the

electronic spins is referred to as the saturation magnetization, or M_s. Once the magnetization is saturated, if the field is decreased back to zero, the magnetization will not return to zero. The material will maintain some net magnetization, called the remnant magnetization, M_r. In order for the magnetization to return to zero, a field must be applied in the opposite direction. The field at which the moments of the domains are again in different directions and the magnetostatic energy is minimized is called the coercivity, H_c. The full cycle of the magnetic field can be achieved by saturating the magnetization in the opposite direction, -M_s, going through the zero field resulting in a remnant magnetization in the opposite direction, -M_r, and increasing the field until $M = 0$, corresponding to -H_c. When the magnetization is once again saturated in the initial direction the hysteresis loop is complete (Cullity 1972).

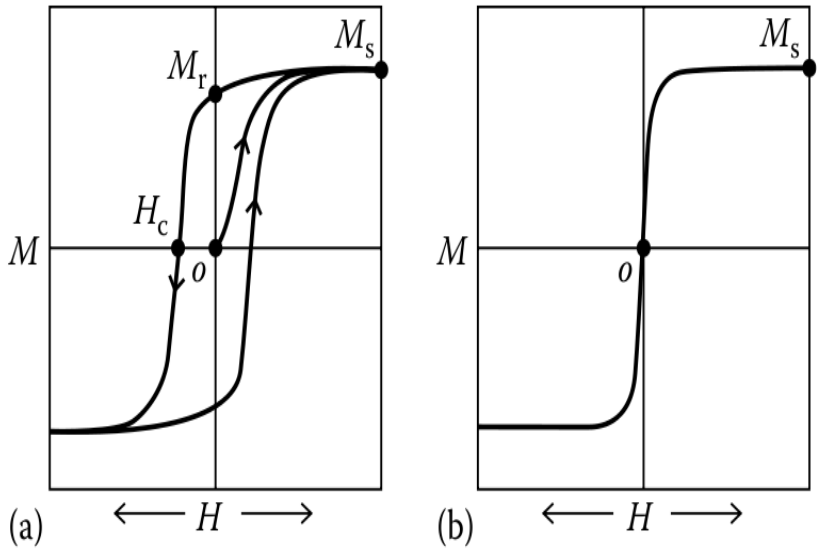


Figure 2.1: Magnetization versus field ($Mvs.H$) curves for (a) an assembly of ferromagnetic nanoparticles and (b) an assembly of superparamagnetic nanoparticles.

OR The Hysteresis loops of Figure 2.1 are plotted as follow (Figure 2.2) :

Materials used in magnetic information storage are chosen based on their values of the parameters described above. The magnetic components of a disk drive are the read

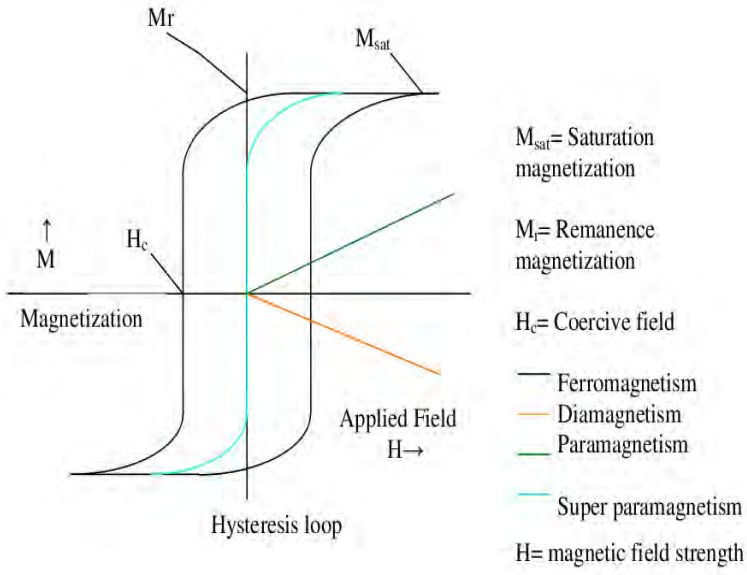


Figure 2.2: Hysteresis loops (magnetization versus applied magnetic field strength) characteristic of ferromagnetic and super paramagnetic nanoparticles.

head, the write head, and the media. The media, which is the focus of this chapter, stores data based on the two stable magnetic configurations corresponding to M_r and -M_r on the hysteresis loop. The stability of the media can be evaluated based on the magnetic anisotropy of the material used. The anisotropy energy, E_A, describes the amount of energy required to reverse the magnetization from one stable state to the other. This depends on several factors, most importantly the effective anisotropy constant,K. The magnetic anisotropy is positively correlated with the coercivity, which is often used to provide a qualitative estimate of the anisotropy of the material, since direct measurements of K can be difficult. In terms of magnetic stability, the more energy that is required to randomize the electronic spins either thermally or via an applied field, the less likely that the information stored in the media will be erased due to stray magnetic fields or excess heat. Therefore, the quest to find better-performing materials to make up hard disk media is centered upon the tailoring of the anisotropy, and thus, the coercivity of the candidate materials.

At odds with the search for high-coercivity materials is the concurrent desire for higher-density data storage. Being able to store data in an ever-decreasing amount of space to continue device miniaturization leads one correctly to conclude that the smaller the magnetic bit, the higher the density of data can be stored within a given amount of space. To that end, it would seem that magnetic nanoparticles would be an obvious choice for the next generation of magnetic data storage. However, analogous to nanoparticles of other functional materials, the size of magnetic nanoparticles encroaches upon a fundamental physical length scale in magnetism, namely the size of a magnetic domain. Like bulk ferromagnets, an array of magnetic nanoparticles containing only one domain (henceforth single domain) can exhibit hysteresis in the magnetization versus field dependence as well (Stoner and Wohlfarth 1949). The key difference between the magnetic behavior of a bulk magnetic material and a collection of single-domain ferromagnetic nanoparticles arises from the mechanism by which the magnetization is cycled through the hysteresis loop. Since domain wall movement is not possible, only coherent magnetization rotation can be used to overcome the effective anisotropy of the particle. Thus, the maximum coercivity of a given material as a function of particle diameter actually falls in the single-domain range.

The critical diameter for a magnetic particle to reach the single-domain limit is expressed as

$$R_{SD} = \frac{36\sqrt{AK}}{\mu_0 M_s^2} \tag{2.1.1}$$

where

$D_{cr} = 2R_{SD}$, D_{cr} = critical diameter

A is the exchange constant

K is the effective anisotropy constant

M_s is the saturation magnetization

For most magnetic materials, this diameter is in the range $10 - 100$nm, though for some high-anisotropy materials the single-domain limit can be several hundred nanometers

(Skomski and Coey 1999).

For a single-domain particle, the amount of energy required to reverse the magnetization over the energy barrier from one stable magnetic configuration to the other is proportional to KV/k_BT, where V is the particle volume, k_B is Boltzmanns constant, and T is the temperature. If the thermal energy is large enough to overcome the anisotropy energy, the magnetization is no longer stable and the particle is said to be superparamagnetic. That is, an array of nanoparticles each with its own moment can be easily saturated in the presence of a field, but the magnetization returns to zero upon removal of the field as a result of thermal fluctuations (i.e., both M_r and Hc are zero). Figure 2.1 is a schematic of the typical shape of (a) an $Mvs.H$ curve for an array of single domain, ferromagnetic nanoparticles (which is qualitatively similar to a bulk ferromagnet) and (b) an array of superparamagnetic nanoparticles. This superparamagnetic behavior is analogous to conventional paramagnets, only, instead of individual electronic spins displaying this fluctuating response, it is the collective moment of the entire particle, and hence the term superparamagnetism. The temperature at which the thermal energy can overcome the anisotropy energy of a nanoparticle is referred to as the blocking temperature, T_B. For an array of nanoparticles with a distribution in volume, T_B represents an average characteristic temperature and can be affected by interparticle interactions as well as the timescale over which the measurement is performed due to the magnetic relaxation of the particles. Keeping these caveats in mind,T_B, as the general transition from ferromagnetism to superparamagnetism, is one of the most important quantities that define the magnetic behavior of an assembly of particles.

2.1.2 Superparamagnetism

Consider an assembly of fine particles, each with an anisotropy energy density E given by $E = KVsin^2\theta$, where K is the uniaxial anisotropy constant , V is the particle volume and θ is the angle between saturation magnetization M_s and the easy axis. In order to reverse the magnetization, a particle must overcome the energy barrier $\Delta E = KV$ where V is the particle volume. When the size of a single domain particle is small enough, spontaneous reversal of magnetization occurs due to the thermal energy K_BT even in the absence of an applied field.

In a typical paramagnet the applied field will help moments to align in the direction of field, and thermal energy will tend to misalign them. This is the characteristic behavior of a normal paramagnetic material in which the magnetic moment under consideration is due to an ion or an atom and is usually a few Bohr magnetons. If a single domain particle is small enough such that the energy barrier KV is comparable to thermal energy K_BT, then this particle behaves like a paramagnet except it has a large moment. As an example a $10\mathring{A}$ spherical particle of iron contains 45 atoms, which gives the moment of $100\mu_B$ (moment of $2.2\mu_B$ per atom). Compared to an atom, the magnetic moment of such a fine particle is huge. Although the behavior of this particle system is similar to a paramagnetic material, it is called superparamagnet due to its large individual particle moment.

Consider an assembly of non-interacting particles each with magnetic moment μ without any directional preference. The magnetization in the presence of an applied field H is explained by the classical theory of paramagnetism since there is no quantization requirement on individual particle moment. Using the classical statistical physics calculation one can show that the magnetization M of this assembly of particles at temperature T with magnetic field H is give by $M = M_sL(a)$, where $M_s = n\mu$ is the saturation magnetization, μ is the magnetic moment of each particle, n is the number of particles per unit volume, and $L(a)$ is the Langevin function ($L(a) = \frac{M}{\mu n} = cotha - \frac{1}{a}$)of $a = \frac{\mu H}{K_BT}$. It is important to

point out that magnetization curves at different temperatures superimpose when M/M_s is plotted as a function of $\frac{\mu H}{K_B T}$. Also if we sweep the field back and forth the same curve of $Mvs.H$ is obtained indicating lack of hysteresis.

One can apply the above theory to small particles when the particle size is so small that thermal energy $K_B T$ is much larger than KV.

2.1.3 Relaxation Time

Consider an assembly of single domain particles. In the presence of an applied field, the particles approach an initial magnetization. Let the field is turned off at time $t = 0$. The particles with thermal energy greater than anisotropy energy KV reverse their magnetization and net magnetization begins to decrease. The time rate of magnetization change will be directly proportional to the existing magnetization M at that time and to the Boltzmann factor $e^{-KV/k_B T}$. The Boltzmann factor is the probability of a particle that has enough energy to surmount the energy barrier $\Delta E = KV$ in order to reverse its magnetization.

$$-\frac{dM}{dt} = f_0 M e^{-KV/k_B T} \tag{2.1.2}$$

Negative sign shows that the magnetization decreases with the time.
The proportionality constant f_0 is known as frequency factor and is about $10^9 sec^{-1}$. Equation 2.1.2 may be written as,

$$-\frac{dM}{dt} = \frac{M}{\tau} \tag{2.1.3}$$

where τ is constant and is known as relaxation time.

$$\frac{1}{\tau} = f_0 e^{-KV/k_B T} \tag{2.1.4}$$

Relaxation time τ is dependent on the volume of the particle and temperature from Equation 2.1.4.

2.1.4 Blocking Temprature (T_B)

Consider an example of spherical cobalt particles of diameter $68\mathring{A}$. The relaxation time at room temperature is calculated by substituting, $K = 45 \times 10^5 ergs/cm^3$, $V = \frac{4}{3}\pi R^3 = 16.45 \times 10^{-20} cm^3$, $f_0 = 10^9 sec^{-1}$, and $T = 300K$ in equation (2.1.4) $\tau = 10^{-1} sec.$ Since the relaxation time is very small, the particles approach thermal equilibrium or zero magnetization in a very short time. Such behavior is the case for superparamagnetism that was discussed above in which KV is much smaller than $k_B T$. If the particle size increases to $90\mathring{A}$, the relaxation time jumps to 3.2×10^9 sec. Since τ is very large, the particles will remain stable for a longer time with fixed initial value of M_r . The above calculations show that a small change in particle size makes a large change in relaxation time.

To calculate the upper limit of volume V_p for superparamagnetic behavior, let the relaxation time of stable behavior be $100sec.$ From Equation (2.1.4).

$$10^{-2} = 10^9 e^{-\frac{KV_P}{K_B T}}$$

$$KV_P = 25 K_B T \tag{2.1.5}$$

Uniform size particles are characterized by a temperature T_B, called blocking temperature, below which particles are stable and ferromagnetic and above which are unstable and superparamagnetic. We consider $\tau = 100sec$ that yields

$$T_B = \frac{KV}{25 K_B} \tag{2.1.6}$$

From the knowledge of upper limit particle size for superparamagnetism T_B can be calculated

Figure 2.3 shows the critical diameter D_p of spherical cobalt particle versus temperature T and which state that cube of D_p is proportional to temperature. Similarly Figure 2.3 represents the relaxation time τ of cobalt particles versus temperature where τ varies

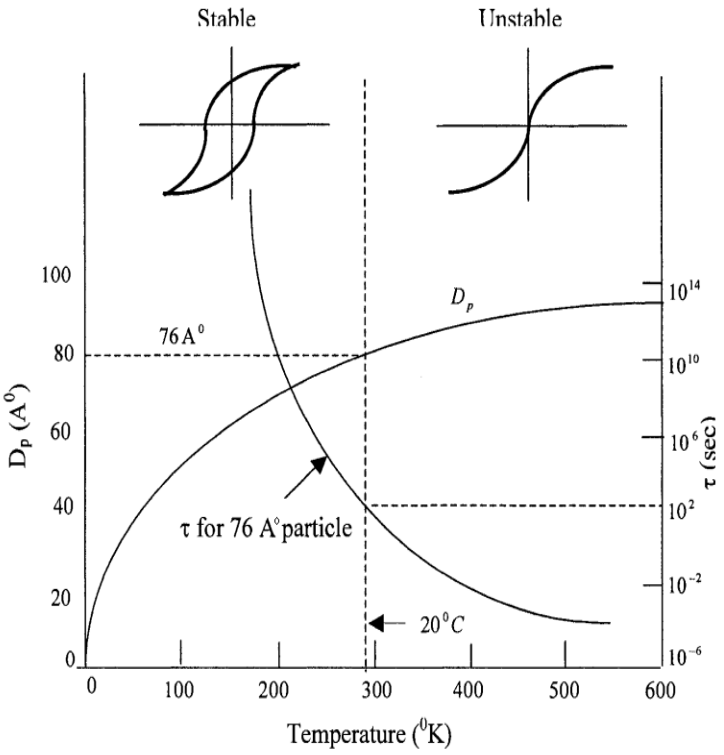


Figure 2.3: Temperature variation of the relaxation time and of critical diameter for spherical cobalt particles.

exponentially with temperature and is given by Equation (2.1.4). The variation of critical diameter with temperature shows that 20^0C is the blocking temperature for $7.6nm$ particle diameter. At 20^0C , the relaxation time is $100sec$. Below T_B and above $100sec$, the particles are stable. Above T_B and below $100sec$, the particles become unstable.

2.2 The Importance Of Nanomagnetism

Ever since the beginnings of electronic data processing, new discoveries made by basic science in the field of magnetism have continued to drive spectacular advances in the performance of data storage systems. Progress in nanomagnetism and spintronics promises to take these advances even further.

Data storage has been one of the major applications of magnetism for more than a century. In magnetic material,an item of information can be recorded by locally orienting the magnetisation in either of its two possible directions to form a binary storage system. Recording is the area of applied magnetism in which technological progress has been most spectacular over the last 50 years. This is especially true since the first computer hard drive arrived in 1956. Since then the storage capacity of hard drives has continued growing at an average rate of 45% a year, in half a century producing an increase in storage density of 8 orders of magnitude (300 bits / cm^2 in 1956, 50 billion bits / cm^2 in 2007) . Correspondingly, the size of each data bit has continued to fall, from 0.3 mm $\times$ 1.2mm in 1956 to 25nm $\times$ 80 nm in 2007 .Thus magnetism, like many other areas of physics, has come down to the nanometre scale. Several factors have made this progress possible. First, at the pure science level, a more thorough understanding of certain magnetic phenomena specific to this scale, e.g. instabilities in magnetisation linked to thermal fluctuations, and the evolution of magnetic properties when the lateral dimension of the system becomes comparable to or less than certain lengths characteristic of magnetism. Enormous progress has also been made in the development of magnetic materials for both writing and reading data. New data storage support media have been devised, and others are under development. Thus in a few years, instead of storing information on continuous magnetic layers, we shall be using media composed of arrays of nanometric-scale magnetic dots, each of which will carry one or more data bits. Magnetoresistive materials have been

designed to read data. These materials use properties associated with the spin of electrons, i.e. their intrinsic magnetic moment, and make it possible to produce ultrasensitive magnetic field sensors able to read the magnetic field on the surface of a hard disk and extract the information written there.

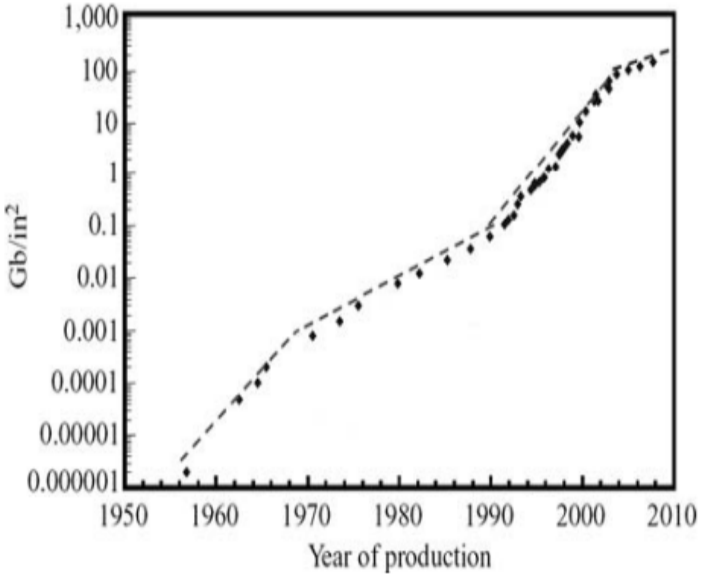


Figure 2.4: Evolution of magnetic recording: hard disk areal density in gigabits per square inch as a function of the year in which the products became available in the market [13]. (Reprinted from [11] with permission from IBM Technical Journals)

Industrial applications of thin films

In the year of discovery of the GMR effect, an initial concept for using the GMR effect in magnetic recording was disclosed [24]. For recording materials one of the most important issues is the areal density of a recording media. It defines how much information can be stored within a certain volume of a recording media. The areal density (normally expressed as billions of bits per square inch of disk surface area, $Gbits/in^2$) is the product of linear density (bits of information per inch of track) multiplied by track density (tracks per inch) [25]. In order to increase the areal density the size of the bits can be decreased. However, it will lead to the smaller writing fields. The challenge is to obtain the more sensitive reading/writing heads which could detect smaller recorded bits and read these

bits at higher data rates.

Using reading heads based on the GMR effect, it was possible to achieve an areal density beyond 100 $Gbyte/in^2$. Such reading heads are based on the magnetic tunnel junction (MTJ). It consists of two ferromagnetic layers separated by an isolator as it is shown in Fig.2.5. The magnetization of the bottom most layer (pinned layer) is fixed by the close contact with the

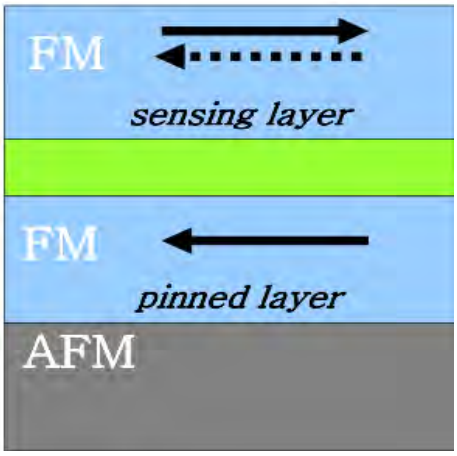


Figure 2.5: The concept of the magnetic tunnel junction

antiferromagnetic layer due to the exchange biasing. The magnetization of the top most layer (sensing layer) is able to change direction even in small magnetic fields. Therefore, depending on the applied magnetic fields the configuration of pinned and sensing layers will be changed from ferromagnetic to antiferromagnetic. Such change will lead to the different tunneling current depending on the magnetic field (see Fig.2.6). This phenomenon is called tunneling magnetoresistance (TMR).

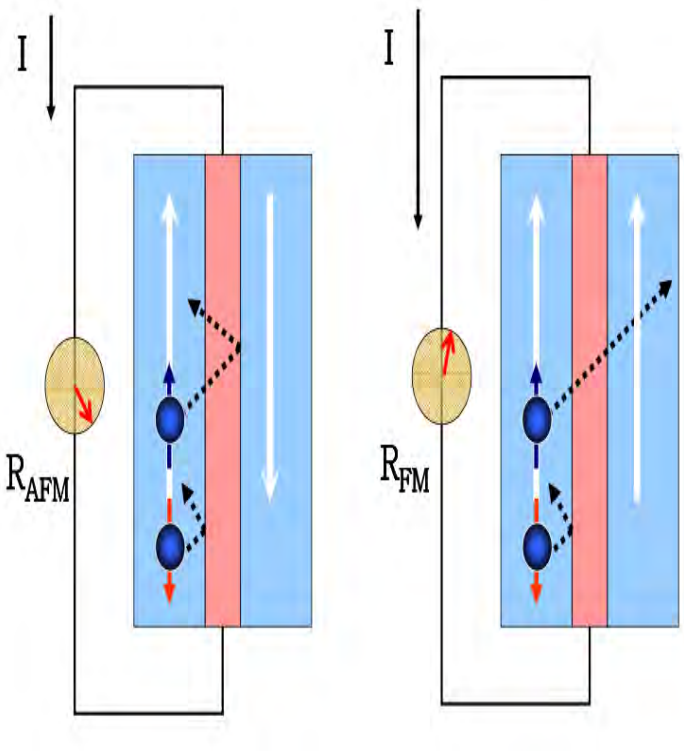


Figure 2.6: The principle of the TMR effect. For the antiferromagnetic configuration of the magnetic layers $R_{AFM} \gg R_{FM}$

Earths Magnetic Field:

Earth has a robust magnetic field due to the presence of charged particles moving within the mantle and cores. This magnetic field protects us from ionizing radiation in the solar wind [27].(see fig 2.7)

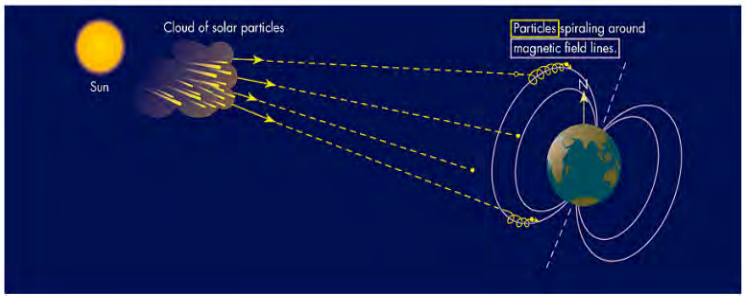


Figure 2.7: Courtesy of Tom Arny, Explorations

Chapter 3

Mathematical Calculation of Nanomagnetic Parameters

3.1 Critical Behavior Of Pure Ferromagnetic Nanoparticles

By using the Gibbs free energy variational principle based on the Bogoliubov inequality the magnetic properties and critical behavior of metallic nanoparticles having concurrently atomic disorder, dilution and competing interactions, are studied within the framework of an Ising model. As a case of study we have considered the $Fe_{0.5}Mn_{0.1}Al_{0.4}$ alloy characterized for exhibiting, under bulk conditions, low temperature reentrant spin glass (RSG) behavior and for which experimental and simulation results are available. Our results allow concluding that the variational model is successful in reproducing features of the dependence of the critical temperature with particle size and low temperature magnetization reduction consistent with a RSG behavior. In this work we compute the magnetization per site and the magnetic susceptibility, as a function of temperature, for different values of the coordination number.

3.1.1 Theoretical Model

Several features lead us to consider an Ising model: i) magnetic frustration can be better resolved with an Ising model than, for instance, with continuous spin models , ii) it is in agreement with the framework we are interested in, which consists of nanoparticles with a single easy axis and agrees also with the relatively high magnetocrystalline anisotropy of the cubic crystalline structure of the alloy considered, iii) it has been already used in similar systems and quite good agreement with experimental data has been achieved, and finally iv) it allows to keep computational requirements under reasonable limits. Thus, our model is based on the following N spins Ising Hamiltonian:(we have used an Ising Model for N Spin with nearest-neighbor interactions described by Hamiltonian):

$$H = -\sum_{\langle ij \rangle} J_{ij}\sigma_i\sigma_j - h\sum_{i=1}^{N}\sigma_i \tag{3.1.1}$$

The first sum runs over nearest neighbors $\langle i, j\rangle$ and σ_i takes on the values ± 1 or 0 depending on whether the i-th site is occupied by a magnetic atom (Fe,Mn) or an aluminum one, respectively. The exchange integral J_{ij} obeys the following probability distribution function accounting for disorder and the different couplings involved :

$$P(J_{ij}) = P^2\delta(J_{ij} - J_{Fe-Fe}) + 2px\delta(J_{ij} - J_{Fe-Mn}) + x^2\delta(J_{ij} - J_{Mn-Mn}) + (q^2 + 2xq + 2pq)\delta(J_{ij}) \tag{3.1.2}$$

where p, x and q, with p + x + q = 1, are the fractional concentrations of Fe, Mn and Al atoms, respectively. The terms p^2, $2px$ and x^2 are the probabilities of having nearest neighbors Fe-Fe, Fe-Mn and Mn-Mn bonds (For high enough iron contents, a RSG behavior within the ferromagnetic phase ruled out by the Fe matrix can arise . whereas the $Mn - Mn$ bonds are antiferromagnetc . On the other hand, the aluminum atoms are considered as non-magnetic and they play the role of magnetic holes in the system causing the dilution effect .), respectively, and interacting through the corresponding exchange

integrals J_{Fe-Fe}, J_{Fe-Mn} and J_{Mn-Mn}. Here, J_{Fe-Fe}, here after simply J, was set to 12.846 meV only for pure iron nanoparticles with body-centered cubic (bcc) structure, and was set to 16.872 meV for $Fe_{0.5}Mn_{0.1}Al_{0.4}$ nanoparticles having the same structure. These values reproduce the critical Curie temperatures of both systems under bulk conditions and the difference among them is attributed to the presence of both Mn and Al atoms and to the fact that Fe and $Fe_{0.5}Mn_{0.1}Al_{0.4}$ have different lattice parameters . Additionally, for the alloy, the remaining exchange integrals were set to $J_{Fe-Mn} = -\alpha J$ and $J_{Mn-Mn} = -\lambda J$ with $\alpha = 0.005$ and $\lambda = 0.03$, and they correspond to the so-called competitive parameters. In this work, such values are kept fixed regardless the size of the nanoparticles to be , considered. The last coefficient $q^2 + 2xq + 2pq$ stands for diluted bonds, with $J_{ij} = 0$, corresponding to nearest neighbors Al-Al, Al-Mn and Al-Fe pairs. Finally, the second term in Eq.(3.1.1) is the Zeeman contribution dealing with the coupling of the spins with a uniform external applied magnetic field h.

Following the ideas proposed by Ferreira et al. , in the pairs approximation, the system is considered as formed by n_1 single spins (S) and n_2 linked pairs (P) of spins with a total number of spins $N = n_1 + 2n_2$. Additionally, it is assumed that the magnetization can be obtained either from single spins or spins belonging to a pair. Thus, the trial Hamiltonian can be written as:

$$H_0 = -\gamma_s \sum_{i \in s} \sigma_i - \sum_{i,j \in p} [J_{ij}\sigma_i\sigma_j + \gamma_p(\sigma_i + \sigma_j)] \tag{3.1.3}$$

where γ_s and γ_p are variational parameters which can be interpreted as molecular fields to be determined from energy minimization conditions. Here, the first sum runs over single spins and the second sum runs over pairs. Both Hamiltonians, Eqs.(3.1.1) and (3.1.3), can be related through the variational approach based on the Bogoliubov inequality:

$$[F] \leq [F_0] + [\langle H - H_0 \rangle_0] \equiv [\Phi] \tag{3.1.4}$$

Where F is the Helmholtz free energy defined by H, F_0 is the free energy defined by H_0 ; $\langle \ldots \rangle_0$ refers to the thermal average in the ensemble defined by H_0, whereas $[\ldots]$ represents

a configurational average in which atomic disorder is considered. According to the way as the system has been figured out we have:

$$F_0 = -K_B T \ln Z_0 = -K_B T \ln(Z_s^{N-2n_2} Z_p^{n_2}) \tag{3.1.5}$$

where

$$Z_0 = \sum_{\{\sigma\}} e^{(-\beta H_0)} \tag{3.1.6}$$

and

$$Z_s = 2cosh(\beta\gamma_s), \tag{3.1.7}$$

$$Z_p = 2e^{\beta J_{ij}} cosh(2\beta\gamma_p) + 2e^{-\beta J_{ij}}, \tag{3.1.8}$$

are the trial partition functions for single(isolated) and pair spins, respectively and $\beta = (K_B T)^{-1}$. The configurational average of any observable A is obtained from:

$$[A] = \int_{\{J_{ij}\}} AP(J_{ij}) dJ_{ij}, \tag{3.1.9}$$

Calculation of the quantities $[F_0]$, $[\langle H - H_0 \rangle_0]$ and $[\Phi]$ has been described as follow the configurational average of F_0 ,to be replace in equation (3.1.4), is caculated from

$$[F_0] = \int_{\{J_{ij}\}} F_0 P(J_{ij}) dJ_{ij}, \tag{3.1.10}$$

By using distribution function given by Eq.(3.1.2), we get

$$\begin{aligned} [F_0] = \quad & -K_B T(N - 2n_2) \ln Z_s - n_2 K_B T\{p^2 \ln Z_P(J) \\ & + x^2 \ln Z_p(-\lambda J) + 2px \ln Z_p(-\alpha J) \\ & + (q^2 + 2pq + 2qx) \ln Z_p(0)\} \end{aligned} \tag{3.1.11}$$

from the thermal average $\langle H - H_0(\gamma)\rangle_0$, we obtain

$$\langle H - H_0(\gamma_s,\gamma_p)\rangle_0 = -J_{ij}m^2\left(\frac{Nz}{2} - n_2\right) - Nhm + (N-2n_2)\gamma_s m + 2n_2\gamma_p m, \tag{3.1.12}$$

where z is the coordination number (z=8 for a bcc lattice), and where we have assumed that the spins are statistically independent, so that $\langle\sigma_i\sigma_j\rangle = m^2$. By doing the configurational average over Eq.(3.1.12), we obtain

$$[\langle H - H_0\rangle_0] = -\left(\frac{Nz}{2} - n_2\right)(p^2 - \lambda x^2 - 2\alpha px)Jm^2 - Nhm + (N-2n_2)\gamma_s m + 2n_2\gamma_p m, \tag{3.1.13}$$

there for $[\Phi]$ can be rewritten as:

$$\begin{aligned}[\Phi] = \quad & -K_BT(N-2n_2)\ln Z_s - n_2K_BT\{p^2\ln Z_P(J) \\ & + x^2\ln Z_p(-\lambda J) + 2px\ln Z_p(-\alpha J) \\ & + (q^2 + 2pq + 2qx)\ln Z_p(0)\} \\ & - \left(\frac{Nz}{2} - n_2\right)(p^2 - \lambda x^2 - 2\alpha px)Jm^2 - Nhm \\ & + (N-2n_2)\gamma_s m + 2n_2\gamma_p m\end{aligned} \tag{3.1.14}$$

leads to the following expression for energy minimization:

$$\begin{aligned}\frac{\partial[\Phi]}{\partial m} = & -2(n' - n_2)(p^2 - 2px\alpha - \lambda x^2)Jm \\ & - Nh + (N-2n_2)\gamma_s + 2n_2\gamma_p = 0\end{aligned} \tag{3.1.15}$$

Where n' is the number of nearest neighbors, which depends on the crystalline structure, the type of boundary conditions and the system size. As concerns to nanoparticles we consider free boundary conditions. Since $[\Phi]$ diminishes as n_2 increases, we take n_2 as large as physically possible, i.e. $n' = n_2$. Thus, the number of linked pairs is maximized. Hence

we obtain the following relationship between the variational parameters or molecular fields γ_s and γ_p:

$$\gamma_s = \frac{(2\gamma_p n'/N) - h}{(2n'/N) - 1} \tag{3.1.16}$$

Our system is a spherical nanoparticle composed by N atoms arranged in a bcc structure with core coordination number z = 8 and interatomic spacing b, which in the case of pure iron is around 2.86 Å whereas for $Fe_{0.5}Mn_{0.1}Al_{0.4}$ is around 2.96 Å . On the basis of such representation and in order to get an expression for the maximum number of pairs divided by the total number of atoms, i.e. n'/N, or, analogously an effective coordination number $z_{eff} = 2n'/N$, we have simulated particles with bcc structure and different diameters D, in units of the lattice parameter b, and have counted the number of nearest neighbors pairs. Figure 3.1 shows the size dependence of z_{eff} from which the following relationship is fulfilled for $D \geq 2$:

$$z_{eff} = \frac{2n'}{N} = z - \frac{b}{D} \tag{3.1.17}$$

where $z = 8$ and the best fit yields $b = 10.13 \pm 0.04$ for a bcc lattice. In the case of a face centered cubic (fcc) lattice, the following values must be used, $z = 12$ and $b = 12.65 \pm 0.06$. In principle, z_{eff} can be interpreted as an effective coordination number for nanoparticles of diameter D whose core coordination number is z. Thus,

the relationship between the molecular fields s and p can be rewritten as:

$$\gamma_s = \frac{\gamma_p z_{eff} - h}{z_{eff} - 1} \tag{3.1.18}$$

Magnetization can be computed either from single spins or from spins linked to a pair, and it must be the same:

$$m = \frac{1}{\beta}\frac{\partial \ln Z_s}{\partial \gamma_s} = \frac{1}{2\beta}\frac{\partial \ln Z_p}{\partial \gamma_p}, \tag{3.1.19}$$

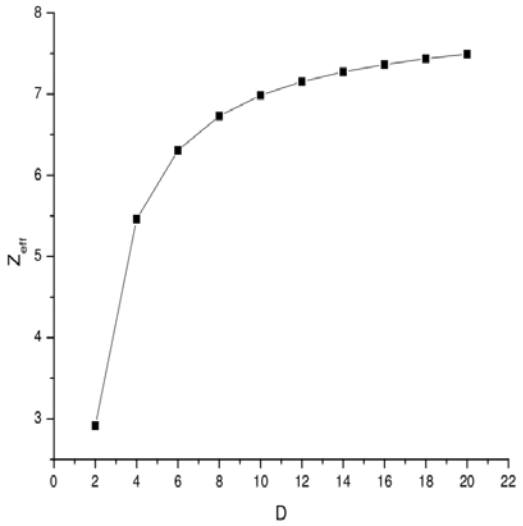


Figure 3.1: Size dependence of the effective (Eq.(3.1.17)) . Particle diameter D is given in units of the lattice parameter b.

After calculating the derivatives and performing the configurational averages using the bonds probability distribution function given by Eq.(3.1.2), we obtain the following transcendental equation for the magnetization:

$$\begin{aligned} m &= tanh(\beta\gamma_s) \\ &= sinh(2\beta\gamma_p)\Bigg[\frac{p^2}{cosh(2\beta\gamma_p)+e^{-2\beta J}} \\ &+\frac{2px}{cosh(2\beta\gamma_p)+e^{2\alpha\beta J}} \\ &+\frac{x^2}{cosh(2\beta\gamma_p)+e^{2\lambda\beta J}}+\frac{q^2+2pq+2qx}{cosh(2\beta\gamma_p)+1}\Bigg] \end{aligned} \tag{3.1.20}$$

Roots of this equation were obtained by using the Find- Root tool of $Mathematica^{\text{TM}}$. It must be stressed that such magnetization, according to the bonds distribution function in Eq.(3.1.2), corresponds to an average magnetization per bond whereas for the pure case (p=1) becomes a magnetization per site. The presence of crossed terms involving the atomic concentrations of the constituent elements p, x and q in Eq.(3.1.20) reflects the average over all possible nearest neighbors pairs as well as the random atomic distribution feature. Zero field magnetic susceptibility was obtained according to $\chi = \left(\frac{\partial m}{\partial h}\right)_0$, yielding:

$$\chi_p = \left(\frac{\partial m}{\partial h}\right)_0 = cosh(2\beta\gamma_p)\frac{2\beta}{z_{eff}}\left[\frac{p^2}{cosh(2\beta\gamma_p)+e^{-2\beta J}}\right.$$
$$+\frac{2px}{cosh(2\beta\gamma_p)+e^{2\alpha\beta J}}$$
$$\left.+\frac{x^2}{cosh(2\beta\gamma_p)+e^{2\lambda\beta J}}+\frac{q^2+2pq+2qx}{cosh(2\beta\gamma_p)+1}\right]$$
$$-sinh^2(2\beta\gamma_p)\frac{2\beta}{z_{eff}}\left[\frac{p^2}{(cosh(2\beta\gamma_p)+e^{-2\beta J})^2}\right.$$
$$+\frac{2px}{(cosh(2\beta\gamma_p)+e^{2\alpha\beta J})^2}$$
$$\left.+\frac{x^2}{(cosh(2\beta\gamma_p)+e^{2\lambda\beta J})^2}+\frac{q^2+2pq+2qx}{(cosh(2\beta\gamma_p)+1)^2}\right] \tag{3.1.21}$$

$$\chi_s = \left(\frac{\partial m}{\partial h}\right)_0 = \frac{\beta}{1-z_{eff}}sech^2(\beta\gamma_s) \tag{3.1.22}$$

The calculation of the Curie temperature T_C from Eq. (3.1.20), for which $m = 0$, is performed by taking the limits $\gamma_p \to 0$ and $\gamma_S \to 0$. This yields the following expression for the magnetic phase diagram:

$$\frac{z_{eff}}{2(z_{eff}-1)} = \frac{p^2}{1+e^{-2\beta_C J}} + \frac{2px}{1+e^{2\alpha\beta_C J}} + \frac{x^2}{1+e^{2\lambda\beta_C J}} + \frac{q^2+2pq+2qx}{2} \tag{3.1.23}$$

Here $\beta_C = (K_B T_C)^{-1}$.

The particular case of pure ferromagnetic nanoparticles is easily obtained by setting p = 1, q = 0 and x = 0 in Eq.(3.1.23):

$$K_B T_C(D) = \frac{2J}{\ln[z_{eff}/(z_{eff}-2)]} \tag{3.1.24}$$

The Temperature dependence of both the magnetization per site and magnetic susceptibility for $\alpha - Fe$ nanoparticles and bulk iron are plotted in Fig. 3.2 .

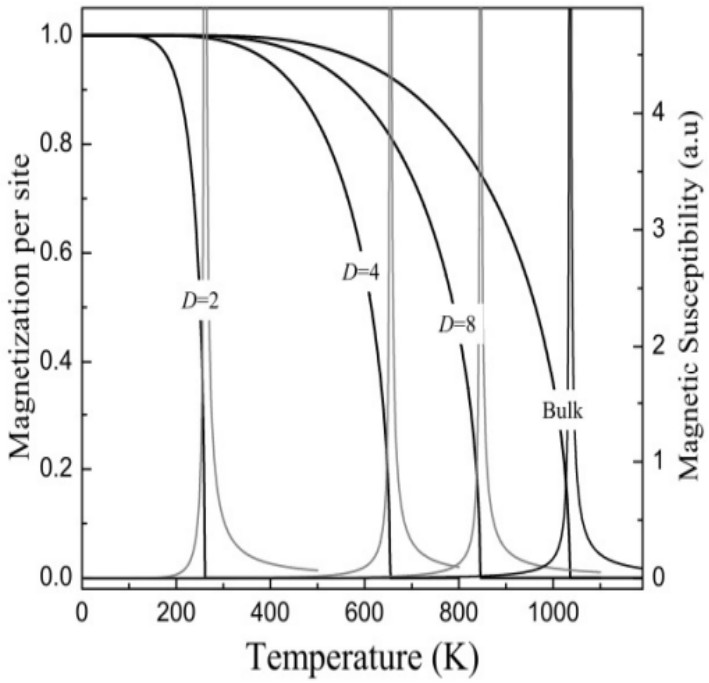


Figure 3.2:

3.1.2 Coordination number

From the particle size dependence of z_{eff} plotted in Fig. 3.1, particles with diameter D=10 (around 3 nm) already exhibit an effective coordination number around 7, which corresponds roughly to 88 % of that of the bulk. Above $D = 10$, the effective coordination number resembles that of the system under bulk conditions. Below that value, coordination number decreases rapidly and, therefore, strong modifications on the magnetic properties are expected to occur in this range, i.e. below around 3 nm. In order to gain a deeper insight on the interpretation of z_{eff}, we have computed the coordination number per particle z_i by counting the number of nearest neighbors surrounding the atom at the i^{th} position, i.e. within the first coordination shell, and an average coordination number was computed according to:

$$\langle z \rangle = \frac{1}{N} \sum_{i=1}^{N} n_i z_i \tag{3.1.25}$$

where n_i is the number of atoms having coordination number z_i (see Fig.3.3). Hence, what we have called an effective coordination number can indeed be considered as an average coordination number, i.e. $z_{eff} = \langle z \rangle$. For diameters below around 2b the average coordination number is characterized by jumps for which the discrete character of the system becomes more evident. A typical particle with D =10 is illustrated in Fig.3.3, where surface atoms with different coordinations are depicted.

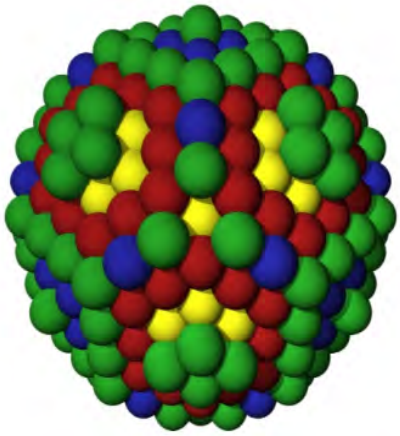


Figure 3.3: (Color online) Particle with diameter D =10 having 1067 atoms, bcc structure, and an average coordination number $\langle z \rangle = 6.96$. Surface atoms with 4, 5, 6 and 7 nearest neighbors are colored green, blue, red, and yellow, respectively

3.1.3 $T_C(D)$ of Pure nanoparticles

The particular case of pure ferromagnetic nanoparticles is easily obtained by setting p =1,q = 0 and x = 0 in Eq.(3.1.23):

$$K_B T_C(D) = \frac{2J}{\ln[z_{eff}/(z_{eff} - 2)]} \tag{3.1.26}$$

Which gives the particle size dependence of the Curie temperature for nanoparticles with core coordination z, diameter D and a nearest neighbors exchange integral J. We want to stress that these results are not exclusively applicable to pure $\alpha - Fe$ nanoparticles and they can be, in principle, employed for other pure ferromagnetic nanoparticles like

Ni or Co. We can also relate this critical temperature with that of the system under bulk conditions in order to obtain a reduced critical temperature:

$$\frac{T_C(D)}{T_C(\infty)} = \frac{J(D)\ln[z/(z-2)]}{J(\infty)\ln[z_{eff}/(z_{eff}-2)]}, \tag{3.1.27}$$

where we have assumed that the exchange integral (J = J(D)) in the nanoparticle can be different from that under bulk conditions ($J(\infty)$). In a first order of approximation

$$\left[\text{ Note : natural logarithm (ln) series} \right.$$

$$\ln x = \frac{x-1}{x} + \frac{1}{2}\left[\frac{x-1}{x}\right]^2 + \frac{1}{3}\left[\frac{x-1}{x}\right]^3 + ...\left(x > \frac{1}{2}\right) \quad \left. \right]$$

, and by assuming the same exchange integral value, which could be reasonable for high enough particle sizes, we have:

$$\frac{T_C(D)}{T_C(\infty)} \approx \frac{z_{eff}}{z}, \tag{3.1.28}$$

if we assume that no structural transition occurs as a consequence of reducing the size. Otherwise, different core coordination numbers should be considered and the model is still applicable. Figure (3.4) shows the reduced critical temperature for different diameters according to our model.

As is observed, from equation (3.1.26),(3.1.27) and (3.1.28) Curie temperature (T_C) decreases as the particle becomes smaller due basically to the decrease in the magnetic bonds density. Therefore, the energy cost to carry out the transition is lower, and thus the critical temperature is also smaller. As D increases the critical temperature T_C tends to its bulk value. [26]

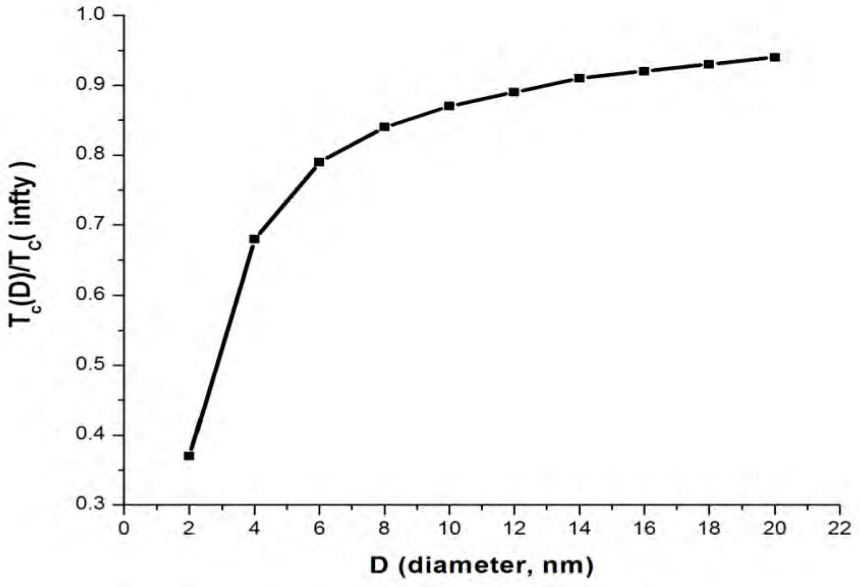


Figure 3.4: Particle size dependence of the reduced critical temperature for pure ferromagnetic nanoparticles with z=8 ,according to Eqs.(3.1.28) .

3.1.4 Graphic Representation Of $T_C(D)$

$$T_C(D) = \frac{2J}{K_B \ln[Z_{eff}/(Z_{eff}-2)]} \tag{3.1.29}$$

where

$Z_{eff} = \frac{2n'}{N} = Z - \frac{b}{D}$

$K_B = 1.38 \times 10^{-23} JK^{-1}, J = joul$

= Boltzmann constant , D = diameter

for bcc ,$Z = 8, b = 10.13 \pm 0.04 = 10.17, 10.09$

for fcc ,$Z = 12, b = 12.65 \pm 0.06 = 12.71, 12.59$

$J = 12.846$ meV , for Fe (pure nanoparticles)

$= 20.579292 \times 10^{-22} J \approx 20.58 \times 10^{-22} J$

$J = 16.872$ meV , for $Fe_{0.5}Mn_{0.1}Al_{0.4}$ (nanoparticles)

$= 27.028944 \times 10^{-22} J \approx 27.03 \times 10^{-22}$J

1meV $= 10^{-3} \times 1.602 \times 10^{-19}$J , 1 Joul $= 10^7$erg

$T_C(D)$ = Curie temprature of nanopareticles

J = exchange integral or exchange energy

Z = coordination number , Z_{eff} = effective coordination number

$$T_C(D) = \frac{2J}{K_B \ln[Z - \frac{b}{D}/((Z - \frac{b}{D}) - 2)]} \tag{3.1.30}$$

For example

For pure iron nanoparticles of bcc structure with different diameter (D),the values of $T_C(D)$ are :

D = 2nm

$$T_C(2) = \frac{2 \times 20.58 \times 10^{-22} J}{1.38 \times 10^{-23} JK^{-1} \ln[8 - \frac{10.17}{2}/((8 - \frac{10.17}{2}) - 2)]} = 257.410K$$

D = 4nm

$$T_C(4) = \frac{2 \times 20.58 \times 10^{-22} J}{1.38 \times 10^{-23} JK^{-1} \ln[8 - \frac{10.17}{4}/((8 - \frac{10.17}{4}) - 2)]} = 653.443K$$

D = 6nm

$$T_C(6) = \frac{2 \times 20.58 \times 10^{-22} J}{1.38 \times 10^{-23} JK^{-1} \ln[8 - \frac{10.17}{6}/((8 - \frac{10.17}{6}) - 2)]} = 781.676K$$

D = 8nm

$$T_C(8) = \frac{2 \times 20.58 \times 10^{-22} J}{1.38 \times 10^{-23} JK^{-1} \ln[8 - \frac{10.17}{8}/((8 - \frac{10.17}{8}) - 2)]} = 845.582K$$

D = 10nm

$$T_C(10) = \frac{2 \times 20.58 \times 10^{-22} J}{1.38 \times 10^{-23} JK^{-1} \ln[8 - \frac{10.17}{10}/((8 - \frac{10.17}{10}) - 2)]} = 883.876K$$

D = 12nm

$$T_C(12) = \frac{2 \times 20.58 \times 10^{-22} J}{1.38 \times 10^{-23} JK^{-1} \ln[8 - \frac{10.17}{12}/((8 - \frac{10.17}{12}) - 2)]} = 909.388K$$

D = 14nm

$$T_C(14) = \frac{2 \times 20.58 \times 10^{-22} J}{1.38 \times 10^{-23} JK^{-1} \ln[8 - \frac{10.17}{14}/((8 - \frac{10.17}{14}) - 2)]} = 927.602K$$

D = 16nm

$$T_C(16) = \frac{2 \times 20.58 \times 10^{-22} J}{1.38 \times 10^{-23} JK^{-1} \ln[8 - \frac{10.17}{16}/((8 - \frac{10.17}{16}) - 2)]} = 941.259K$$

D = 18nm

$$T_C(18) = \frac{2 \times 20.58 \times 10^{-22} J}{1.38 \times 10^{-23} JK^{-1} \ln[8 - \frac{10.17}{18}/((8 - \frac{10.17}{18}) - 2)]} = 951.879K$$

D = 20nm

$$T_C(20) = \frac{2 \times 20.58 \times 10^{-22} J}{1.38 \times 10^{-23} JK^{-1} \ln[8 - \frac{10.17}{20}/((8 - \frac{10.17}{20}) - 2)]} = 960.373K$$

Table 3.1: Theoretical and Experimental values [22,23] of $T_C(D)$,Z_{eff} and Z_{eff}/Z for different values of D

.

D	2	4	6	8	10	12	14	16	18	20
Z_{eff}	2.92	5.46	6.31	6.73	6.98	7.15	7.27	7.36	7.44	7.49
$T_c(D)_{Cal}$	257	653	782	846	884	909	928	941	951	960
$T_c(D)_{Exp}$	264	662	789	846	887	907	922	930	942	950
Z_{eff}/Z	0.37	0.68	0.79	0.84	0.87	0.89	0.91	0.92	0.93	0.94

In principle, z_{eff} can be interpreted as an effective coordination number for nanoparticles of diameter D whose core coordination number is z. (see fig (3.5))

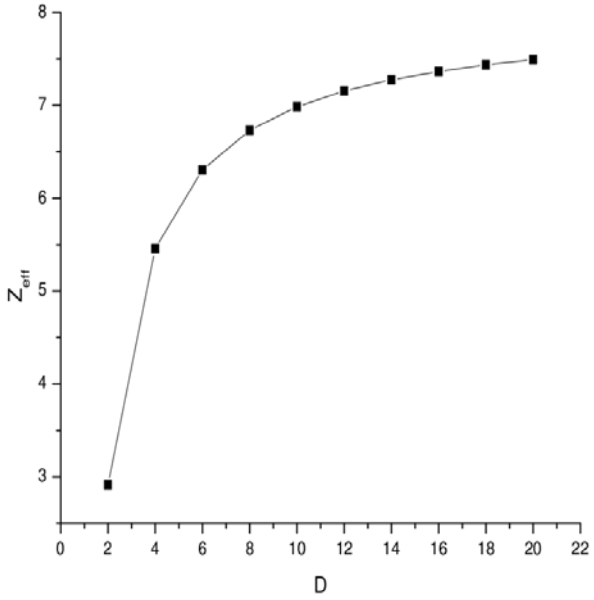


Figure 3.5: Effective coordinate number versus Diameter

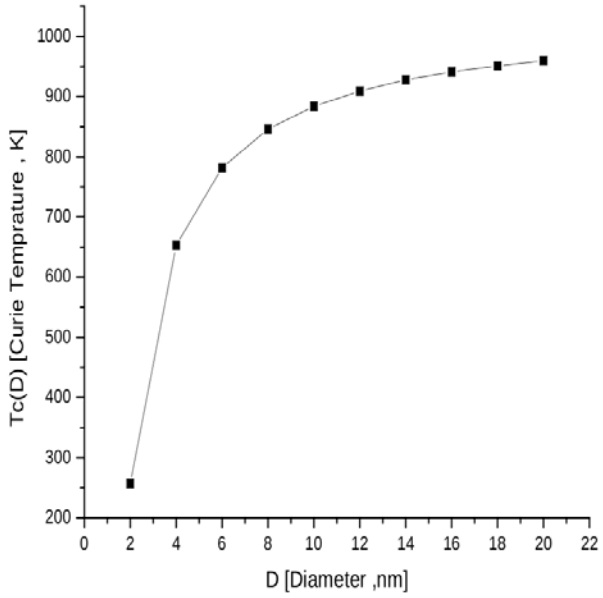


Figure 3.6: $T_C(D)$ versus Diameter

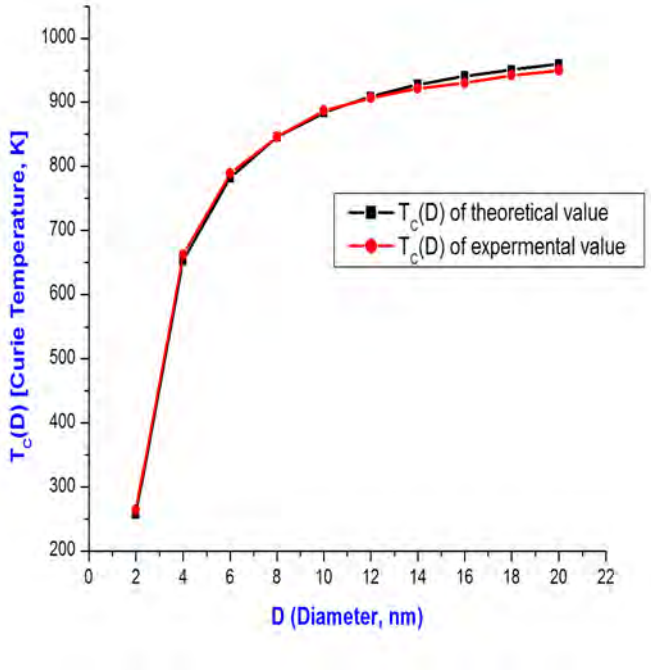


Figure 3.7: $T_C(D)$ versus Diameter

Chapter 4

Result and Conclusion

As is observed, from equation (3.1.26), (3.1.27) and (3.1.28) Curie temperature (T_C) decreases as the particle becomes smaller due basically to the decrease in the magnetic bonds density. Therefore, the energy cost to carry out the transition is lower, and thus the critical temperature is also smaller. As D increases the critical temperature T_C tends to its bulk value.

The key difference between the magnetic behavior of a bulk magnetic material and a collection of single-domain ferromagnetic nanoparticles arises from the mechanism by which the magnetization is cycled through the hysteresis loop.

The effect of dilution and the presence of competing interactions upon the magnetic properties and critical behavior of $Fe_{0.5}Mn_{0.1}Al_{0.4}$ nanoparticles was addressed by means of the standpoint of the free energy variational principle based on the Bogoliubov inequality . In order to validate the use of the former approach to the case of nanoparticles, which is carried out for the first time, the model was applied to account for the critical behavior of pure ferromagnetic nanoparticles. More concretely, the equation yielding the critical ferromagnetic to paramagnetic line is given in terms of an average nearest neighbors coordination number which is particle size dependent. Our results allow to conclude that the model is successful in reproducing features of the dependence of the critical temperature with the particle size.

Reference

[1] G. L. Verschuur, *Hidden attraction: the history and mystery of magnetism*, New York: Oxford University Press, (1993).

[2] J. F. Keithley, *The story of electrical and magnetic measurements*: from 500 BC to the 1940s, New York: IEEE Press, (1999).

[3] J. C. Maxwell, *A Treatise on Electricity and Magnetism*, New York: Dover Publications (1954).

[4] N. Majlis, *The quantum theory of magnetism, Singapore*, River Edge, World Scientific, (2000).

[5] M. P. Marder, *Condensed matter physics*, New York: John Wiley, (2000).

[6] R. Skomski, J. Phys.: Condens. Matter. **15**, R841 (2003).

[7] J. I. Martn, J. Nogus, K. Liu, J. L. Vicent, and I. K. Schuller, J. Magn. Magn. Mater. 256, 449 (2003).

[8] D. C. Jiles, Acta Mater. **51**, 5907 (2003).

[9] C. Alexiou, R. Jurgons, in Magnetic Drug Targeting, ed. by W. Andra, H. Nowak. *Magnetism in Medicine*: A Handbook, 2nd edn. (Wiley, Weinheim, 2007), pp. 596605

[10] M.E. Evans, F. Heller, *Environmental Magnetism* (Academic Press, San Diego, 2003)

[11] G. Fleissner, B. Stahl, P. Thalau, G. Falkenberg, G. Fleissner, Naturwissenschaften **94**, 631642 (2007)

[12] P. P. Freitas, H. Ferreira, S. Cardoso, S. van Dijken, J. Gregg, in Nanostructures for Spin Electronics, ed. by D. Sellmyer, R. Skomski. *Advanced Magnetic Nanostructures* (Springer, New York, 2006), pp. 403460

[13] R.F. Freitas, W.W. Wilcke, IBM J. Res. Dev. **52**, 439447 (2008)

[14] R. Wu, A.J. Freeman, Phys. Rev. Lett. **69**, 28672870 (1992)

[15] R. Hergt, W. Andra , in Magnetic Hyperthermia and Thermoablation, ed. by W. Andra , H. Nowak. *Magnetism in Medicine*: A Handbook, 2nd edn. (Wiley, Weinheim, 2007), pp. 550570

[16] J. Jorzick, C. Kramer, S. O. Demokritov, B. Hillebrands, B. Bartenlian, C. Chappert, D. Decanini, F. Rousseaux, E. Cambril, E. Sondergard, M. Bailleul, C. Fermon, A.N. Slavin, J. Appl. Phys. **89**, 70917095 (2001)

[17] S. Odenbach, in Ferrofluids, ed. by K.H.J. Buschow. Handbook of Magnetic Materials, vol **16** (Elsevier, Amsterdam, 2006), pp. 127208

[18] S. Ohnishi, A. J. Freeman, M. Weinert, Phys. Rev. B **28**, 67416748 (1983)

[19] S.N. Song, J. Ketterson, in Ultrathin Films and Superlattices, ed. by R.W. Cahn, P. Haasen, E.J. Kramer. Electronic and Magnetic Properties of Metals and Ceramics, vol 3A (Wiley, New York, 1991)

[20] D. Weller, T. McDaniel, in Media for Extremely High Density Recording, ed. by D. Sellmyer, R. Skomski. *Advanced Magnetic Nanostructures* (Springer, New York, 2006), pp. 295324

[21] R. Wiltschko, W. Wiltschko, *Magnetic Orientation in Animals* (Springer, Berlin, 1995)

[22] Blaowang and C.H.Woo J.Apply.Phys . **97**,084109 (2005)

[23] B.wang and C.H.Woo J.Apply.Phys . **94** ,4053 (2003)

[24] P. Grunberg, *Magnetic Field Sensor With Ferromagnetic Thin Layers Having Magnetically Antiparallel Polarized Components*, U.S. Patent 4, 949, 039.

[25] J. Belleson http://www.hitachigst.com

[26] $www.ffn.un, es/oscar/Articles/PRB - 2010 - Velasquez$

[27] $CourtesyofRodNave, http://hyperphysics.phy-astr.gsu.edu/hbase/magnetic/magearth.html$

Declaration

This thesis is my original work, has not been presented for a degree in any other University and that all the sources of material used for the thesis have been dully acknowledged.

Name: Abrham Feseha

Signature:– – – – – – – – – – – –

Place and time of submission: Addis Ababa University, June 2011

This thesis has been submitted for examination with my approval as University advisor.

Name: Prof. P.Singh

Signature:– – – – – – – – – ––